Capillary-driven elastic attraction between quantum dots

Kailang Liu, Isabelle Berbezier, Luc Favre, Antoine Ronda, Marco Abbarchi, Patricia Donnadieu, Peter W Voorhees, Jean-Noël Aqua

▶ **To cite this version:**

Kailang Liu, Isabelle Berbezier, Luc Favre, Antoine Ronda, Marco Abbarchi, et al.. Capillary-driven elastic attraction between quantum dots. Nanoscale, 2019, 11 (16), pp.7798-7804. 10.1039/c9nr00238c . hal-02348666

HAL Id: hal-02348666
https://hal.science/hal-02348666

Submitted on 10 Nov 2019

HAL is a multi-disciplinary open access archive for the deposit and dissemination of scientific research documents, whether they are published or not. The documents may come from teaching and research institutions in France or abroad, or from public or private research centers.

L'archive ouverte pluridisciplinaire **HAL**, est destinée au dépôt et à la diffusion de documents scientifiques de niveau recherche, publiés ou non, émanant des établissements d'enseignement et de recherche français ou étrangers, des laboratoires publics ou privés.

Journal Name

ARTICLE TYPE

Cite this: DOI: 10.1039/xxxxxxxxxx

Capillary-driven elastic attraction between quantum dots.

Kailang Liu,[a] Isabelle Berbezier,[a] Luc Favre,[a] Antoine Ronda,[a] Marco Abbarchi,[a] Patricia Donnadieu,[b] Peter Voorhees,[c] Jean-Noël Aqua,[d]

Received Date
Accepted Date

DOI: 10.1039/xxxxxxxxxx

www.rsc.org/journalname

We present a novel self-assembly route to align SiGe quantum dots. By a combination of theoretical analyses and experimental investigation, we show that epitaxial SiGe quantum dots can cluster in ordered close-packed assemblies, revealing an attractive phenomena. We compute nucleation energy barriers, accounting for elastic effects between quantum dots through both elastic energy and strain-dependent surface energy. If the former is mostly repulsive, we show that the decrease in the surface energy close to an existing island reduces the nucleation barrier. It subsequently increases the probability of nucleation close to an existing island, and turns out to be equivalent to an effective attraction between dots. We show by Monte-Carlo simulations that this effect describes well the experimental results, revealing a new mechanism ruling self-organisation of quantum dots. Such generic process could be observed in various heterogeneous systems and could pave the way to a wide range of applications.

1 Introduction

Quantum dots (QD) were first investigated almost three decades ago for their potential applications in microelectronics[1–3] Recently a renewed interest has been driven in quantum molecules and quantum dots arrays due to local field interactions between interconnected primitive nanoscale logic blocks that could allow to transfer and process digital information[4]. QDs are now commonly manufactured by different techniques, from colloidal synthesis, lithography, 3D printing to epitaxy, and are used for many different purposes in fundamental systems, such as in quantum photonics, lasing or excitonic systems[5–16], and in commercial devices such as screen displays or memories[17–22]. Recently with the renewed interest in quantum dots based quantum information[23–25] it has become highly challenging to self-organize limited assemblies of laterally close packed quantum dots[26–32]. The technique best suited for device integration is epitaxy where quantum dots growth is driven by the elastic relaxation of the misfit strain. Even-though its general picture is rather well documented and understood[33], some puzzling experimental outcomes can still be revealed by careful scrutiny[34–37]. One such experimental finding is the clustering of Ge quantum dots in their early stage of growth on Si[38]. It occurs in the stochastic nucleation regime[39], and can not be related to the partial order of their instability-driven growth[40]. Spatial correlation between islands was not reported in the experimental literature of SiGe systems, see e.g. Ref.[33,41] for reviews. These systems are commonly described by the Stranski-Krastanov growth with non-correlated stochastic nucleation events[42,43]. This clustering reveals a bias in the nucleation process towards an effective attraction between dots. This bias is theoretically counterintuitive given the a priori repulsive behavior of isotropic elastic interactions[44,45]. Elastic interaction between islands[46] was recently shown to correct islands sizes and size distribution. In irreversible growth, the long-range repulsive elastic interactions subsequently favor adatoms to drift away from other adatoms[47,48] and existing islands[49]. In addition, SiGe quantum dots involve more complex phenomena with the presence of a wetting layer[50], reversible aggregation, shape transition and anomalous coarsening[33].

We investigate here a mechanism that can trigger the clustering of quantum dots in homogeneous nucleation. Even if direct elastic interactions are repulsive, we show that the quite sensible strain-dependence of the surface energy enforces a decrease in the surface energy close to an existing island. This decrease introduces *de facto* a reduction of the nucleation barrier which favors the growth of new islands nearby an already grown island.

[a] *Institut Matériaux Microélectronique Nanoscience de Provence, Aix-Marseille Université, UMR CNRS 6242, 13997 Marseille, France.*
[b] *Université Grenoble Alpes, CNRS, Grenoble INP, SIMAP, 38000 Grenoble, France.*
[c] *Department of Materials Science and Engineering, Northwestern University, Evanston, Illinois 60208-3108, USA.*
[d] *Sorbonne Université, CNRS, Institut des Nanosciences de Paris, INSP, UMR 7588, 4 place Jussieu, 75005 Paris, France. E-mail: aqua@insp.jussieu.fr*

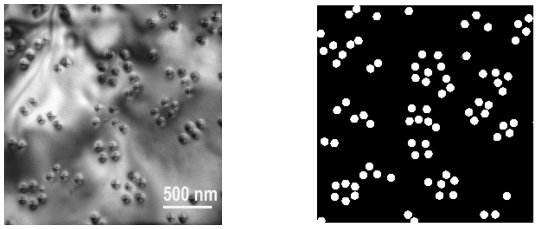

Fig. 1 (left) Low magnification TEM image of Ge islands nucleated on Si(001) and (right) pixelized image enhancing visibility of islands correlation.

To test the amplitude of this effect, we perform Monte-Carlo simulations of a simplified model of nucleation on a lattice. Considering the decrease in the nucleation barrier found energetically, we find a degree of correlation close to experiments, validating the aforementioned origin of clustering.

2 Clustering between islands

We deposited 1 nm pure Germanium by Molecular Beam Epitaxy (MBE) in Ultra High Vacuum on a Silicon (001) substrate heated at 550°C. The substrate temperature is monitored with an optical pyrometer. The Ge flux is obtained from a solid source in an effusion cell heated at 1150°C and is calibrated by RHEED oscillations. A Ge growth rate of 0,016nm/sec is commonly used. A complete description of the experimental protocol can be found in Ref.[38]. The resulting surface with a clear island clustering is given in Fig. 1. It exhibits 3D islands with square based pyramid shapes representative of the so-called 'hut' islands[33]. The mean size of these Ge hut islands is about 45 nm, as already observed previously. It is noticeable that islands align mainly along their faces and sometimes along their corners, while the alignment at large scale does not follow the crystallographic orientations (and neither any specific orientation), see Fig. 2, excluding any elastic anisotropy effect[51,52]. As discussed below, for a larger deposited thickness ($\sim$1.5 nm), a bi-modal size distribution of Ge islands is observed with the coexistence of dome and hut islands. Domes islands result from the merging of hut islands. Their mean size is about 150 nm. But we focus in the following on the narrow regime of parameters where the experiments can be clearly and unambiguously interpreted by an island clustering, with an ordering that can be accurately quantified. Hence, we consider systems with (i) only hut islands, (ii) at a low island density (for a deposited thickness around 1 nm), and (iii) in the high-strain nucleation regime (for a Ge concentration larger than $\sim$ 60%). Indeed, (i) hut-islands have been extensively studied and are fully strained (as confirmed by the absence of MoirÃl' fringes on the TEM image) at opposed to the dome islands which are commonly relaxed ; (ii) a low density allows to have a higher level of correlation, well above the measurement noise ; (iii) the nucleation regime ensures a stochastic process as opposed to the ordering that could arise from the instability at work for low Ge concentration[39].

To quantify the island clustering of Fig. 1, we compute the island correlation function. Correlations between M islands of density ρ are characterized as usual[53] by their radial distribution function $g(r)=1/(M\rho)\int d\boldsymbol{r}'\,\rho^2(\boldsymbol{r}+\boldsymbol{r}',\boldsymbol{r}')$ with the pair density $\rho^2(\boldsymbol{r},\boldsymbol{r}')=\langle n(\boldsymbol{r})n(\boldsymbol{r}')\rangle-\langle n(\boldsymbol{r})\rangle\delta(\boldsymbol{r}-\boldsymbol{r}')$, with the Dirac delta distribution δ and $n(\boldsymbol{r})=\sum_{i=1}^{M}\delta(\boldsymbol{r}-\boldsymbol{R}_i)$ for islands with mass centres $\boldsymbol{R}_i$. We plot in Figure 3 the radial distribution function $g(r)$, with r the distance between islands, corresponding to the experimental results of Fig. 1. It has a clear and significant peak at short distances extending over σ and 2σ, where σ is the mean island diameter. It then displays a flat plateau where islands are no longer correlated. The maximum value of $g(r)$, $g_{max}\simeq 2.6$ is a clear measure of the importance of correlation between these islands.

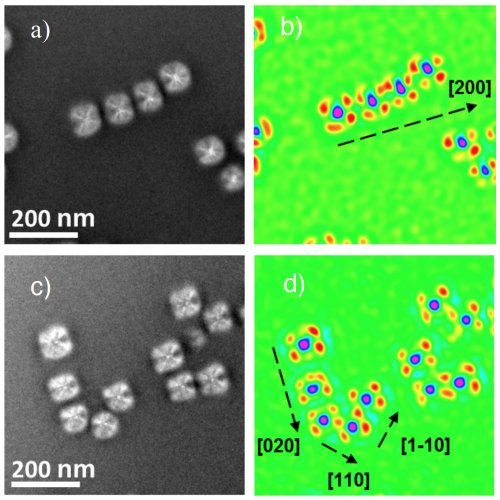

Fig. 2 a) and c) High magnification TEM images of clustering islands. b) and d) retrieved phase maps (method described in[38]) showing the SiGe dots (in blue-purple) and localized strains in their vicinity (in yellow-red).

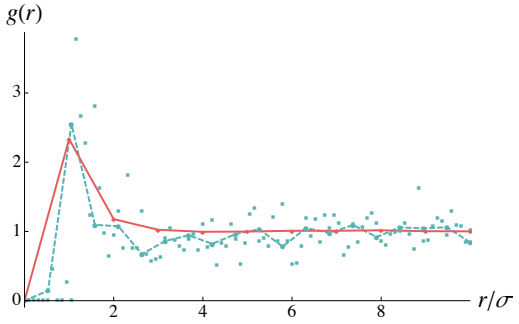

Fig. 3 Radial distribution function $g(r)$ of the islands found experimentally and in Monte Carlo simulations, as a function of their distance r in units of the mean island diameter σ : experimental raw data and average distribution (blue points and dashed-blue line), and simulations (red solid line).

If island clustering is clearly at work in the previous experimental parameters, we also find it in other regimes. We plot in Fig. 4 a large scale image of the island clustering obtained for a deposited thickness of 1.5 nm, all other parameters kept fixed. We now find a bimodal distribution with both hut and dome islands as usually found when increasing the film thickness[33]. Island clustering is again visible to the naked eye, and the the correlation function again displays a maximum at close distance $g_{max}\simeq 2.2$ similar to that of the hut assembly. As the system evolution during growth

This journal is © The Royal Society of Chemistry [year]

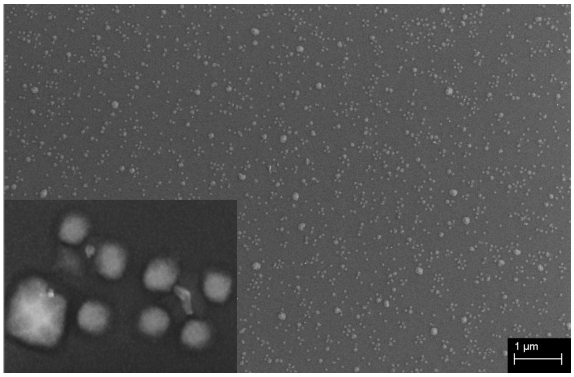

Fig. 4 Scanning electron microscope image of island clustering on a 1.5 nm thick Ge film. Inset, magnification of a cluster with both hut and dome islands.

proceeds mainly by nucleation and coarsening of islands, one may conclude that the correlation found in the initial hut-islands stage do not alter the subsequent growth stages, that inherit the initial islands correlation.

3 Nucleation enhancement

3.1 Model

To rationalize these correlations, we analyse the nucleation at work when pure Ge is deposited[39]. As a first approximation, we consider that islands directly nucleate in (105) square-base pyramids with a side-angle θ *, which greatly simplifies the analysis without significantly altering the following results. The formation energy for the nucleation of a pyramid may be decomposed into surface, elastic and edge energies

$$\Delta E = \Delta E^{surf} + \Delta E^{el} + \Delta E^{edge}, \quad (1)$$

where one has to compute the difference of energy between a flat film of thickness h_0, and pyramids sitting on a wetting layer of thickness $h_w < h_0$ by mass conservation (we consider a formation process where mass is conserved, so that one has a consider $h_0 = h_w + \rho V$ for an island of volume V sitting on an area $1/\rho$).

Elasticity may be computed analytically within the small-slope approximation where the film surface is $z = h_0 + h_1(x,y)$ where h_1 has small slopes. Mechanical equilibrium can be solved exactly in Fourier space and one eventually finds the biaxial strain $\varepsilon(\boldsymbol{r})$ at first order

$$\varepsilon(\boldsymbol{r}) = -m + \zeta\, \mathscr{H}_{ii}[h_1(\boldsymbol{r})], \quad (2)$$

where $\zeta = \dfrac{Y_f(1-\nu_s^2)}{Y_s(1-\nu_f)}$, $\mathscr{H}_{ii}[h_1](\boldsymbol{k}) = |\boldsymbol{k}| h(\boldsymbol{k})$ in Fourier space[54] and $m = (a_s - a_f)/a_s$ is the lattice misfit between the film (f) and substrate (s). We account here for the difference in the film and substrate Young's modulus Y and Poisson's ratio ν that do alter the balance of the energy barrier. We also find the contribution of elasticity to the energy barrier,

$$\Delta E^{el} = -\zeta\, \mathscr{E}_0 \int d\boldsymbol{r}\, h_1(\boldsymbol{r}) \mathscr{H}_{ii}[h_1(\boldsymbol{r})], \quad (3)$$

with the flat-film elastic energy density $\mathscr{E}_0 = Y_f m^2/(1-\nu_f)$ and the misfit m. Note that this integral expression involves the interaction for each point on the surface at $h_1(\boldsymbol{r})$ with the elastic field proportional to $\mathscr{H}_{ii}[h_1(\boldsymbol{r})]$ created by all the other points, that is straightforwardly in Fourier space but that in fact involves a convolution in real space given by an integral over all the surface.

The solution (3) allows to sum up elasticity through a two-dimensional integral, that is computed straightforwardly for different geometries in the following. Considering the small elastic anisotropy in Si/Ge systems, we use here isotropic elasticity † [55].

The capillary contribution may be decomposed into

$$\Delta E^{surf} = \int_{\Delta} d\boldsymbol{r}\, \gamma_{Ge}^{(105)}[\varepsilon(\boldsymbol{r})]/\cos\theta + \int_{\overline{\Delta}} d\boldsymbol{r}\, \gamma_{Ge}^{(001)}[\varepsilon(\boldsymbol{r})] - \gamma_{Ge}^{(001)}[\varepsilon_0]/\rho, \quad (4)$$

where Δ is the in-plane domain where the pyramid sits, and $\overline{\Delta}$, the domain of the wetting layer, and with the SiGe nominal strain $\varepsilon_0 = -4.2\%$. Eq. (4) accounts explicitly for the surface stress via the strain-dependence of the surface energy. The latter was investigated by different first-principles studies [56–59] that give different results for the surface energies. However, their strain dependence that is more important in the subsequent study are similar. Thereafter, we will consider the results from [56], see Fig. 5, with the 2×8 reconstruction that is mainly observed experimentally,

$$\gamma_{Ge}^{(001)}(\varepsilon) = 67.2 + 156.3\,\varepsilon, \quad (5)$$

in meV/Å^2, while for the (105) orientation,

$$\gamma_{Ge}^{(105)}(\varepsilon) = 66.8 + 103.6\,\varepsilon - 1577.8\,\varepsilon^2, \quad (6)$$

that is slightly increased by 0.8meV/Å^2 compared to [56] to avoid a too-low surface energy for the (105) facet. Indeed, if $\gamma_{Ge}^{(105)}/\cos\theta < \gamma_{Ge}^{(001)}$, capillarity would enforce a faceting transition as the surface would spontaneously break up into facets to minimize its surface energy. In order to avoid this facetting transition that is not observed experimentally, we add this small correction, arguing in addition the uncertainty concerning microscopic details such as reconstruction, that would alter surface energies. We thence characterize surface effects through the capillary parameter $\eta = \gamma_{Ge}^{(105)}(\varepsilon_0)/\gamma_{Ge}^{(001)}(\varepsilon_0)\cos\theta - 1$, that is 0.004 from Eqs. (5)-(6). The computation in (4) involves the inhomogeneous strain field $\varepsilon(\boldsymbol{r})$ that can be computed straightforwardly for each geometry thanks to (2). The important feature for the subsequent analysis is that the surface energies Eqs. (5)-(6) decrease when compression increases (decrease of the strain for

* The base L and height H of a square-base pyramid of volume V are $L = \alpha V^{1/3}$ and $H = \frac{1}{2}\alpha \tan\theta\, V^{1/3}$ with $\alpha = (6/\tan\theta)^{1/3}$.

† Even if anisotropy may lead to some attraction in some directions in metallic systems, it can not rationalize the dot clustering under focus that do not show any preferential direction

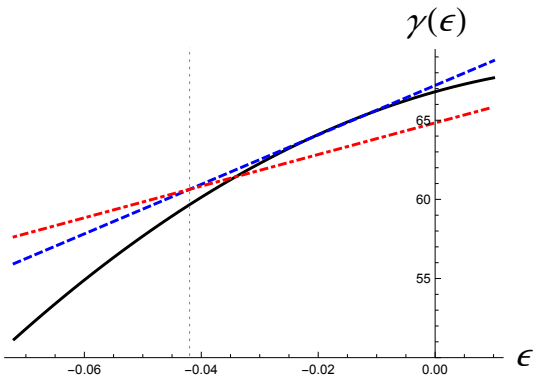

Fig. 5 Strain dependence of the surface energy in meV/Å^2 for the (105) (solid black line) and (001) (blue dashed line for Eq. (5) and red dot-dashed line for the alternative Eq. (7)) orientations. The nominal strain $\varepsilon = -0.042$ is indicated by the vertical dotted line.

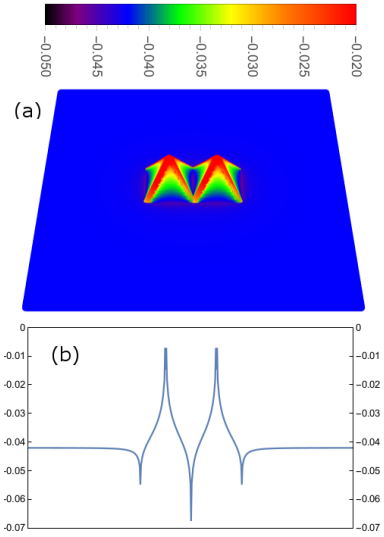

Fig. 6 Strain map $\varepsilon(\boldsymbol{r})$ as given by (2) computed for a surface with two islands.

negative values). Finally, the edge energy is given analytically by $\Delta E^{edge} = \frac{4H}{\tan\theta}\left(2+\sqrt{2+\tan^2\theta}\right)\sigma^{ed}$ for a pyramid of height H, with the edge energy $\sigma^{ed} = 3.3\text{meV/Å}$[39,60,61].

3.2 Inhomogeneous nucleation barrier

The previous ingredients may already qualitatively rationalize the correlation among nucleating dots. We plot in Fig. 6 the strain map on a surface where two islands are close to one another. In between the islands, the absolute value of the strain is maximal as the two islands sum up their compressive strain. This effect is still valid, but with a decreasing amplitude when the islands are pulled away. As the surface-stress results in a decrease in the surface energy as a function of the compressive strain, this region of high strain will decrease the surface energy in between islands, reducing the nucleation barrier and enhancing the nucleation probability. We evaluate this effect by considering a sequential nucleation where an island nucleates in the neighborhood of an already existing island. We compute the change in the energy barrier of nucleation of the second island, as a function of the base-to-base distance between the two islands, see Fig. 7. With the parameters given above and especially in Eqs. (5) and (6), we find that the decrease in the energy barrier is $\delta\Delta E = 0.10$ eV close to an island with a typical critical volume, a value which is already 10% of the single pyramid nucleation barrier $\Delta E = 0.96$ eV. This estimate is noticeably dependent on the different surface energies strain dependence. The literature reveals different first-principles results that are comparable but with still non-negligible differences[56–59]. By changing the slope of the (001) surface energy within this uncertainty, with the alternative

$$\gamma_{Ge}^{(001)}(\varepsilon) = 64.8 + 100\,\varepsilon\,, \tag{7}$$

plotted in Fig. 5, we find that the decrease in the energy barrier can amount to 0.20 eV in this extreme case.

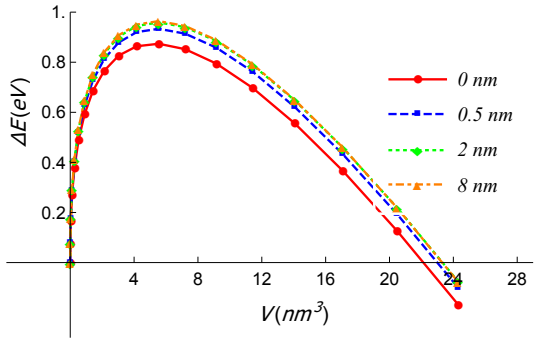

Fig. 7 Energy barrier (1) for nucleation of a new island of volume V close to an already existing island at a base-to-base distance of 0, 0.5, 2 and 8 nm

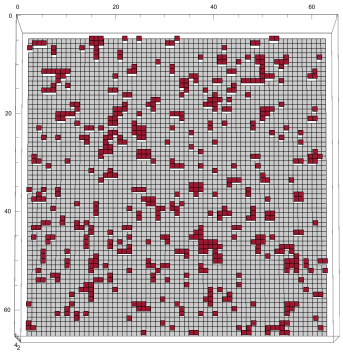

Fig. 8 Kinetic Monte-Carlo simulations of the biased nucleation model

4 Biased nucleation model

To investigate whether the lowering of the nucleation barrier found previously can rationalize the degree of island correlation found experimentally, we devise an ad-hoc model of biased nucleation, with an inhomogeneous nucleation close or far from existing islands. We consider islands that nucleate randomly on a lattice with sites i following a probability p_i per unit time. Once an island has nucleated on a given site, the site is no longer available

This journal is © The Royal Society of Chemistry [year]

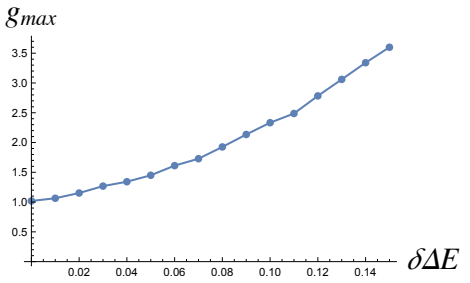

Fig. 9 Maximum of the correlation function in the biased nucleation model as a function of the decrease in the nucleation barrier $\delta\Delta E$ (given in eV).

for further nucleation, thence introducing exclusion effects[62,63]. If a site does not have any nearest-neighbor close to it, the nucleation probability is the reference probability p_0. The nucleation probability on a site with one nearest neighbor is increased by the Boltzmann factor associated with the decrease in the nucleation barrier found previously, $p_0 \exp(\beta\,\delta\Delta E)$ with the inverse temperature $1/k_BT$. As a first approximation, if a site has n_i nearest neighbors, we assume that the influence of the different nearest-neighbors sums up, as does the elastic field in the linear elasticity framework. Hence, the nucleation probability in this case reads $p_0 \exp(\beta\, n_i\, \delta\Delta E)$. As a first approximation, we neglect in this model any kinetic effect on the adatom diffusion nearby an island or adatom depletion.

We evaluate the nucleation statistics resulting from this model using rejection-free kinetic Monte-Carlo (KMC) simulations[64,65]. The statistical properties of the system are parametrized by the mean coverage ϑ measuring the density of occupied lattice sites. In order to compare with the experimental results, we consider a coverage $\vartheta = 13\%$, corresponding to Fig. 1. We use the experimental temperature $T = 550^\circ$C and the nucleation barrier decrease found above, $\delta\Delta E = 0.10$ eV. The resulting surface is plotted in Fig. 8 where island clustering is again evident to the naked eye. The corresponding correlation function is plotted in Fig. 3, where correspondance with experimental result is manifest. Of particular interest is the maximum of the correlation function at the close-contact distance g_{max} that is a quantitative measure of the degree of correlation. With the decrease of 0.10 eV, we find $g_{max} = 2.4$ very close to the 2.6 experimental value in hut islands and 2.5 in hut and dome islands. This correspondance is very good, especially given all the approximations made both in the nucleation model and estimate of the nucleation barrier decrease. In particular, we plot in Fig. 9 the maximum value g_{max} as a function of the decrease in the nucleation barrier. We find that a small change in $\delta\Delta E$ may result in a large increase in g_{max}, showing that the model results are completely within the experimental range of correlation. We therefore argue that the dot clustering found in experiments may fully be rationalized by the surface-stress induced lowering of the nucleation barrier. Extra effects such as alloying, defects[66], anisotropy[67], patterning[68,69] etc, that could also alter the absolute value of the nucleation barrier, will be investigated in future work.

5 Conclusions

Thanks to the combination of experimental and theoretical results, we rationalize the nucleation of correlated Ge quantum dots. Even though elasticity is mainly repulsive, the strain dependence of the surface energy enforces a decrease in the surface energy close to an island. This effect reduces the energy barrier by ~ 0.1 eV for the nucleation of a second island close to an already-grown one. We performed Monte-Carlo simulations of a dedicated model to quantify the effect of such a decrease on the amount of correlation, and found good agreement with the experiments. This work reveals the subtle balance of different effects that trigger the growth mechanisms of nanostructures. It opens the way for further theoretical analysis based on nucleation models accounting neatly for the driving forces, and to experimental investigation in other epitaxial systems.

Conflicts of interest

There are no conflicts to declare.

Notes and references

1 G. Abstreiter, P. Schittenhelm, C. Engel, E. Silveira, A. Zrenner, D. Meertens and W. Jäger, *Semicond. Sci. Technol.*, 1996, **11**, 1521.

2 S. H. Kwok, P. Y. Yu, C. H. Tung, Y. H. Zhang, M. F. Li, C. S. Peng and J. M. Zhou, *Phys. Rev. B*, 1999, **59**, 4980.

3 S. Kanjanachuchai, J. M. Bonar and H. Ahmed, *Semicond. Sci. Technol.*, 1999, **14**, 1065.

4 Y. Ma, T. Zhou, Z. Zhong and Z. Jiang, *J. Semicond.*, 2018, **39**, 061004.

5 M. Bayer, P. Hawrylak, K. Hinzer, S. Fafard, M. Korkusinski, Z. R. Wasilewski, O. Stern and A. Forchel, *Science*, 2001, **291**, 451.

6 G. W. Bryant, M. Zieliński, N. Malkova, J. Sims, W. Jaskólski and J. Aizpurua, *Phys. Rev. B*, 2011, **84**, 235412.

7 L. Monniello, C. Tonin, R. Hostein, A. Lemaitre, A. Martinez, V. Voliotis and R. Grousson, *Phys. Rev. Lett.*, 2013, **111**, 026403.

8 M. Heiss, Y. Fontana, A. Gustafsson, G. Wüst, C. Magen, D. D. O'Regan, J. W. Luo, B. Ketterer, S. Conesa-Boj, A. V. Kuhlmann, J. Houel, E. Russo-Averchi, J. R. Morante, M. Cantoni, N. Marzari, J. Arbiol, A. Zunger, R. J. Warburton and A. Fontcuberta i Morral, *Nature Mater.*, 2013, **12**, 439.

9 Y. Yang, Y. Zheng, W. Cao, A. Titov, J. Hyvonen, J. R. Manders, J. Xue, P. H. Holloway and L. Qian, *Nature Photon.*, 2015, **9**, 259.

10 P. M. Vora, A. S. Bracker, S. G. Carter, T. M. Sweeney, M. Kim, C. S. Kim, L. Yang, P. G. Brereton, S. E. Economou and D. Gammon, *Nature Comm.*, 2015, **6**, 7665.

11 A. Lyasota, S. Borghardt, C. Jarlov, B. Dwir, P. Gallo, A. Rudra and E. Kapon, *J. Cryst. Growth*, 2015, **414**, 192.

12 S. Chen, W. Li, J. Wu, Q. Jiang, M. Tang, S. Shutts, S. N. Elliott, A. Sobiesierski, A. J. Seeds, I. Ross, P. M. Smowton and H. Liu, *Nature Photon.*, 2016, **10**, 307.

13 M. Grydlik, M. T. Lusk, F. Hackl, A. Polimeni, T. Fromherz,

W. Jantsch, F. Schäffler and M. Brehm, *Nano Lett.*, 2016, **16**, 6802.
14 M. Davanco, J. Liu, L. Sapienza, C.-Z. Zhang, J. V. De Miranda Cardoso, V. Varun, R. Mirin, S. W. Nam, L. Liu and K. Srinivasan, *Nature Comm.*, 2017, **8**, 889.
15 M. Schatzl, F. Hackl, M. Glaser, P. Rauter, M. Brehm, L. Spindlberger, A. Simbula, M. Galli, T. Fromherz and F. Schäffler, *ACS Photon.*, 2017, **4**, 665.
16 V. Poborchii, A. Shklyaev, L. Bolotov, N. Uchida, T. Tada and Z. N. Utegulov, *Appl. Phys. Expr.*, 2017, **10**, 125501.
17 E.-S. Hasaneen, E. Heller, R. Bansal, W. Huang and F. Jain, *Solid-State Electronics*, 2004, **48**, 2055.
18 A. G. Nassiopoulou, A. Olzierski, E. Tsoi, I. Berbezier and A. Karmous, *J. NanoSci. NanoTech.*, 2007, **7**, 316.
19 C. B. Simmons, M. Thalakulam, B. M. Rosemeyer, B. J. Van Bael, E. K. Sackmann, D. E. Savage, M. G. Lagally, R. Joynt, M. Friesen, S. N. Coppersmith and M. A. Eriksson, *Nano Lett.*, 2009, **9**, 3234.
20 P. O. Anikeeva, J. E. Halpert, M. G. Bawendi and V. Bulović, *Nano Lett.*, 2009, **9**, 2532.
21 A. Marent, T. Nowozin, M. Geller and D. Bimberg, *Semiconductor Sci. Technol.*, 2011, **26**, 014026.
22 P. Dimitrakis, P. Normand, V. Ioannou-Sougleridis, C. Bonafos, S. Schamm-Chardon, G. BenAssayag and E. Iliopoulos, *Phys Stat. Sol. (a)*, 2013, **210**, 1490.
23 E. Kawakami, P. Scarlino, D. R. Ward, F. R. Braakman, D. E. Savage, M. G. Lagally, M. Friesen, S. N. Coppersmith, M. A. Eriksson and L. M. K. Vandersypen, *Nature Nanotech.*, 2014, **9**, 666.
24 K. Takeda, J. Kamioka, T. Otsuka, J. Yoneda, T. Nakajima, M. R. Delbecq, S. Amaha, G. Allison, T. Kodera, S. Oda and S. Tarucha, *Sci. Adv.*, 2016, **2**, e1600694.
25 M. Russ, D. M. Zajac, A. J. Sigillito, F. Borjans, J. M. Taylor, J. R. Petta and G. Burkard, *Phys. Rev. B*, 2018, **97**, 085421.
26 P. Barthelemy and L. M. K. Vandersypen, *Annal. Phys.*, 2013, **525**, 808.
27 M. Y. Kagan, V. V. Val'kov and S. V. Aksenov, *Phys. Rev. B*, 2017, **95**, 035411.
28 T. Hensgens, T. Fujita, L. Janssen, X. Li, C. J. Van Diepen, C. Reichl, W. Wegscheider, S. Das Sarma and L. M. K. Vandersypen, *Nature*, 2017, **548**, 70.
29 V. Kornich, C. Kloeffel and D. Loss, *Quantum*, 2018, **2**, 70.
30 S. A. Studenikin, L. Gaudreau, K. Kataoka, D. G. Austing and A. S. Sachrajda, *Appl. Phys. Lett.*, 2018, **112**, 233101.
31 C. Jones, M. A. Fogarty, A. Morello, M. F. Gyure, A. S. Dzurak and T. D. Ladd, *Phys. Rev. X*, 2018, **8**, 021058.
32 L. R. Schreiber and H. Bluhm, *Science*, 2018, **359**, 393.
33 J.-N. Aqua, I. Berbezier, L. Favre, T. Frisch and A. Ronda, *Phys. Rep.*, 2013, **522**, 59.
34 J. J. Zhang, G. Katsaros, F. Montalenti, D. Scopece, R. O. Rezaev, C. Mickel, B. Rellinghaus, L. Miglio, S. De Franceschi, A. Rastelli and O. G. Schmidt, *Phys. Rev. Lett.*, 2012, **109**, 085502.
35 G. Ramalingam, J. A. Floro and P. Reinke, *J. Appl. Phys.*, 2016, **119**, 205305.
36 Y. Yamamoto, P. Zaumseil, G. Capellini, M. A. Schubert, A. Hesse, M. Albani, R. Bergamaschini, F. Montalenti, T. Schroeder and B. Tillack, *Nanotechnol.*, 2017, **28**, 485303.
37 T. David, J. Aqua, K. Liu, L. Favre, A. Ronda, M. Abbarchi, J. Claude and I. Berbezier, *Sci. Rep.*, 2018, **8**, 2891.
38 P. Donnadieu, T. Neisius, A. Gouyé, G. Amiard, A. Ronda and I. Berbezier, *J. NanoSci. NanoTech.*, 2011, **11**, 9208.
39 K. Liu, I. Berbezier, T. David, L. Favre, A. Ronda, M. Abbarchi, P. W. Voorhees and J.-N. Aqua, *Phys. Rev. Materials*, 2017, **1**, 053402.
40 J.-N. Aqua, A. Gouyé, A. Ronda, T. Frisch and I. Berbezier, *Phys. Rev. Lett.*, 2013, **110**, 096101.
41 B. Voigtänder, *Surf. Sci. Rep.*, 2001, **43**, 127.
42 A. Vailionis, B. Cho, G. Glass, P. Desjardins, D. G. Cahill and J. E. Greene, *Phys. Rev. Lett*, 2000, **85**, 3672.
43 B. Cho, T. Schwarz-Selinger, K. Ohmori, D. G. Cahill and J. E. Greene, *Phys. Rev. B*, 2002, **66**, 195407.
44 L. Landau and E. Lifchitz, *Theory of Elasticity*, USSR Academy of Sciences, Moscow, USSR, 1986.
45 A. Pimpinelli and J. Villain, *Physics of Crystal Growth*, Cambdrige University Press, 1998.
46 I. I. Izhnin, O. I. Fitsych, A. V. Voitsekhovskii, A. P. Kokhanenko, K. A. Lozovoy and V. V. Dirko, *App. Nanosc.*, 2019, 1.
47 F. Gutheim, H. Müller-Krumbhaar and E. Brener, *Phys. Rev. E*, 2001, **63**, 041603.
48 G. Nandipati and J. G. Amar, *Phys. Rev. B*, 2006, **73**, 045409.
49 R. Grima, J. DeGraffenreid and J. A. Venables, *Phys. Rev. B*, 2007, **76**, 233405.
50 K. A. Lozovoy, A. P. Kokhanenko and A. V. Voitsekhovskii, *Phys. Chem. Chem. Phys.*, 2015, **17**, 30052.
51 V. A. Shchukin and D. Bimberg, *Rev. Mod. Phys.*, 1999, **71**, 1125–1171.
52 M. Meixner, E. Schöll, V. A. Shchukin and D. Bimberg, *Phys. Rev. Lett.*, 2001, **87**, 236101.
53 D. A. Mc Quarrie, *Statistical Mechanics*, Harper Collins, New York, 1976.
54 J.-N. Aqua, T. Frisch and A. Verga, *Phys. Rev. B*, 2007, **76**, 165319.
55 B. Croset, H. Guesmi and G. Prévot, *Phys. Rev. B*, 2007, **76**, 073405.
56 O. E. Shklyaev, M. J. Beck, M. Asta, M. J. Miksis and P. W. Voorhees, *Phys. Rev Lett.*, 2005, **94**, 176102.
57 G.-H. Lu and F. Liu, *Phys. Rev. Lett.*, 2005, **94**, 176103.
58 G.-H. Lu, M. Cuma and F. Liu, *Phys. Rev. B*, 2005, **72**, 125415.
59 D. Scopece, F. Montalenti and M. J. Beck, *Physical Review B*, 2012, **85**, 085312–.
60 C. M. Retford, M. Asta, M. J. Miksis, P. W. Voorhees and E. B. Webb, *Phys. Rev. B*, 2007, **75**, 075311.
61 K. A. Lozovoy, A. P. Kokhanenko and A. V. Voitsekhovskii, *Crystal Growth & Design*, 2015, **15**, 1055–1059.
62 J.-N. Aqua and M. E. Fisher, *Phys. Rev. Lett.*, 2004, **92**, 135702.

This journal is © The Royal Society of Chemistry [year]

63 M. E. Fisher, J.-N. Aqua and S. Banerjee, *Phys. Rev. Lett.*, 2005, **95**, 135701.
64 A. B. Bortz, M. H. Kalos and J. L. Lebowitz, *J. Comput. Phys.*, 1975, **17**, 10.
65 P. Gaillard, J.-N. Aqua and T. Frisch, *Phys. Rev. B*, 2013, **87**, 125310.
66 I. Goldfarb, P. T. Hayden, J. H. G. Owen and G. A. D. Briggs, *Phys. Rev. Lett.*, 1997, **78**, 3959.
67 J.-N. Aqua, A. Gouyé, T. Auphan, T. Frisch, A. Ronda and I. Berbezier, *Appl. Phys. Lett.*, 2011, **98**, 161909.
68 J. N. Aqua and X. Xu, *Phys. Rev. E*, 2014, **90**, 030402.
69 J.-N. Aqua and X. Xu, *Surf. Sci.*, 2015, **639**, 20.